

# Diurnal Patterns in the Observed Cloud Liquid Water Path Response to Droplet Number Perturbations

Kevin M. Smalley<sup>1</sup>, Matthew D. Lebsock<sup>1</sup>, and Ryan Eastman<sup>2</sup>

<sup>1</sup>Jet Propulsion Laboratory, California Institute of Technology, Pasadena, California, USA

<sup>2</sup>Department of Atmospheric Sciences, University of Washington, Seattle, Washington, USA

## Key Points:

- The adjustment of cloud liquid water path to aerosols in stratocumulus clouds is generally negative, except for the thickest clouds.
- There is a strong diurnal cycle in the adjustment of cloud liquid water path to aerosols.

## Abstract

A key uncertainty in Aerosol-cloud interactions is the cloud liquid water path (LWP) response to increased aerosols ( $\lambda$ ). LWP can either increase due to precipitation suppression or decrease due to entrainment-drying. Previous research suggests that precipitation suppression dominates in thick clouds, while entrainment-drying prevails in thin clouds. The time scales of the two competing effects are vastly different, requiring temporally resolved observations. We analyze 3-day Lagrangian trajectories of stratocumulus clouds over the southeast Pacific using geostationary data. We find that clouds with a LWP exceeding  $200 \text{ g m}^{-2}$  exhibit a positive response, while clouds with lower LWP show a negative response. We observe a significant diurnal cycle in  $\lambda$ , indicating a more strongly negative daytime adjustment driven by entrainment-drying. In contrast, at night, precipitation suppression can occasionally fully counteract the entrainment-drying mechanism. The time-integrated adjustment appears weaker than previously suggested in studies that do not account for the diurnal cycle.

## Plain Language Summary

We examine how aerosols affect cloud properties, specifically cloud liquid water path (LWP). We find that the impact of aerosols on LWP varies with cloud thickness and time of day. Thicker clouds are more influenced by entrainment-drying during the day and precipitation suppression at night, while thinner clouds that are less likely to precipitate and tend to produce less intense precipitation are much more susceptible to entrainment drying no matter time of day. Overall, this nuanced understanding of how LWP responds to aerosols may help constrain the influence of aerosol-cloud-interactions on climate.

## 1 Introduction

The effective radiative forcing from cloud-aerosol interactions ( $\text{ERF}_{ACI}$ ) in marine boundary layer clouds are a leading source of uncertainty in future climate projections (Mülmenstädt & Feingold, 2018; Seinfeld et al., 2016). These uncertainties result from ambiguity in how individual cloud properties (i.e. cloud liquid water path (LWP), cloud fraction, and cloud drop size) adjust to aerosols (e.g. Christensen et al., 2020; Douglas & L'Ecuyer, 2020). Whereas the sensitivity of cloud drop size to aerosol perturbation is fairly well understood (Twomey, 1977), the response of LWP and cloud fraction is less well constrained. In particular, LWP adjustment can follow two pathways: 1) LWP may

increase due to suppressed precipitation following the second-indirect aerosol effect in more polluted environments (Albrecht, 1989) or 2) LWP may decrease in response to more efficient entrainment-drying near cloud top (Ackerman et al., 2004; Bretherton et al., 2007). The relative magnitude of both processes significantly affects aerosol impacts on cloud radiative properties.

The sensitivity of LWP to changes in cloud droplet number concentration is quantified as  $\lambda = \frac{d \ln LWP}{d \ln N_d}$ . Previous high-resolution large-eddy simulation (LES) and observational studies generally agree that  $\lambda$  is positive in precipitating clouds but negative in non-precipitating clouds (e.g. Ackerman et al., 2004; Fons et al., 2023; Glassmeier et al., 2021; Gryspeerd et al., 2022; Hill et al., 2009; Lebsock et al., 2008; Lee et al., 2009; Michibata et al., 2016; Prabhakaran et al., 2023; Toll et al., 2019). The implication of this finding is that the  $ERF_{ACI}$  is largest in regimes that tend to produce precipitation, whereas regimes that tend not to produce precipitation tend to have an  $ERF_{ACI}$  that is less than the Twomey effect (Twomey, 1977). To visualize this, Equation 1 shows how albedo ( $A_c$ ) changes with  $N_d$  in response to changes in  $\lambda$  (Boers & Mitchell, 1994; Platnick & Twomey, 1994). This shows that  $\lambda$  needs to be less than -0.4 to fully counteract the Twomey effect. Interestingly, Qiu et al. (2023) and Zhou and Feingold (2023) observed  $\lambda$  values below -0.4 in thick non-precipitating and the smallest closed-cell stratocumulus. These findings, while intriguing, represent exceptions compared to most estimates, which rarely fall below -0.4. This suggests that the negative adjustment due to entrainment-drying often falls short of fully countering the Twomey Effect.

$$\frac{dA_c}{dN_d} = \frac{A_c(1 - A_c)}{3N_d} \left( 1 + \frac{5}{2}\lambda \right) = \begin{cases} \text{Brightening} & \text{if } \lambda > -0.4 \\ \text{Darkening} & \text{if } \lambda < -0.4 \end{cases} \quad (1)$$

Adding to the complexity of interpreting  $\lambda$  is the diurnal cycle of both entrainment and precipitation in stratocumulus. Of note, Diamond et al. (2020) compared morning  $\lambda$  estimated from the Moderate Resolution Imaging Spectroradiometer (MODIS) onboard Terra to afternoon  $\lambda$  estimated from MODIS onboard Aqua within the southeast Atlantic shipping corridors. They found that  $\lambda$  generally becomes more negative from morning to afternoon, implying that the influence of entrainment-drying on LWP increases throughout the day. From an LES perspective, Sandu et al. (2008) found that LWP increases at night and decreases during the day, with diurnal changes being much larger

in the most polluted environments. Their diurnal cycle in LWP sensitivity coincides with the diurnal cycle in stratocumulus precipitation, which peaks before sunset and generally decreases throughout the day (Burleyson et al., 2013). Based on this limited evidence, one could speculate that a diurnal cycle of  $\lambda$  that is modulated by the diurnal cycle of precipitation may exist. The observed magnitude of  $\lambda$  and its potential diurnal cycle may shed light on the practicality of marine-cloud brightening - a proposed solar radiation management strategy (Diamond et al., 2022; Hoffmann & Feingold, 2021; Prabhakaran et al., 2023; Wood, 2021). However, comprehensive observations are necessary to validate this hypothesis.

Given that  $\lambda$  may change throughout the day, and the time-scale of the adjustment is on the order 20 hours Glassmeier et al. (2021), using polar-orbiting satellites for analysis limit our ability to provide observational constraints on the diurnal cycle of  $\lambda$ . Previous studies have developed innovative techniques to make inferences about  $\lambda$  using MODIS measurements from Terra and Aqua. For instance, Gryspeerdt et al. (2022) identified a weak LWP- $N_d$  relationship that is highly dependent on the initial cloud state. However, a limitation is that Terra and Aqua provide only two data points at a given location every 24 hours, and those samples are limited to two discrete times of day. To address this limitation, Christensen et al. (2023) combined geostationary satellite observations with polar orbiters and ground-based stations to quantify  $\lambda$  in the U.S. Department of Energy’s Energy Exascale Earth System Model. Consistent with other research, they found that  $\lambda$  is typically negative during the day. However, their approach used geostationary observations to track changes in cloud state, rather than directly measuring LWP. In our study, we employ a combination of geostationary LWP dataset that has been corrected for scattering geometry related biases and microwave imagery which is insensitive to solar geometry to assess the diurnal variations of  $\lambda$ .

## 2 Data and Methods

### 2.1 Corrected ABI Cloud Liquid Water Path

We use cloud-optical depth ( $\tau$ ) and cloud-top effective radius ( $r_e$ ) pixels retrieved from the liquid-only (Pavolonis, 2020) GOES-16 Advanced-Baseline Imager (ABI) (Walther & Straka, 2020) from 2019 to 2021 (downloaded from NOAA CLASS; <https://www.class.noaa.gov>) to calculate low-cloud LWP using equation 17 from (Grosvenor et

al., 2018) for solar zenith angles  $< 70^\circ$ . This method assumes an adiabatic increase in liquid-water content with height and a constant number concentration. We apply the corrections described in Smalley and Lebsock (2023a) to mitigate the scattering geometry bias, which are ubiquitous features of bi-spectral cloud microphysical retrievals. These corrections adjust the LWP over a  $1^\circ \times 1^\circ$  degree area to that which would be observed by that of microwave imagers, that do not suffer scattering biases. Smalley and Lebsock (2023a) demonstrate that the corrected ABI LWP is able to reproduce the diurnal cycle of LWP observed by the fleet of microwave imagers but with the benefit of the 10-minute temporal resolution of ABI.

## 2.2 Microwave Cloud Liquid Water Path

For solar zenith angles  $> 70^\circ$ , we supplement the corrected daytime ABI data with LWP derived from the passive microwave imagers listed in Table S1. These data are downloaded from Remote Sensing Systems (RSS; <https://www.remss.com>). RSS utilizes 37-GHz brightness temperatures for each satellite to derive LWP at a resolution of  $0.25^\circ \times 0.25^\circ$ , employing the same algorithm and calibration procedure (e.g. Wentz, 1997; Wentz & Spencer, 1998) to mitigate biases between sensors. Five of the six satellites are sun-synchronous but have varying equatorial-crossing times. This, in conjunction with the Global Precipitation Measurement Microwave Imager (which operates in a processing orbit), enables us to sample throughout the nocturnal portion of the diurnal cycle. To ensure the use of LWP data in regions free from potential bias caused by ice clouds or precipitation, we follow the procedure described by Smalley and Lebsock (2023a).

## 2.3 MODIS Cloud Droplet Number Concentration

We use cloud droplet number derived from the level-2 Terra and Aqua MODIS collection 6.1 cloud product optical depth and effective radius at  $2.1 \mu\text{m}$  (Platnick et al., 2015) co-located with GOES-16. Although number concentration from MODIS and ABI are based on similar theoretical bases, Figure S1 shows that ABI has a significant low bias relative to lidar observations (Hu et al., 2021), that MODIS does not have. We speculate that the bias in the ABI data relates to the larger footprint of the ABI compared to MODIS and the presence of ABI effective radii larger than  $30 \mu\text{m}$  which is the cut-off value for the MODIS retrieved liquid  $r_e$ .

## 2.4 Lagrangian Analysis

Following Smalley et al. (2022), we generate trajectories initiated from every 50 MODIS pixels during each Terra overpass. To focus the results on Stratocumulus conditions, trajectories are filtered for initial conditions with an estimated inversion strength (Wood & Bretherton, 2006) greater than 9.5 K. The median initial cloud fraction of these trajectories is 80%, which is consistent with the Stratocumulus cloud type. We calculate the average initial  $N_d$  within a  $1^\circ \times 1^\circ$  gridbox around each trajectory point from the MODIS pixel level optical depth and effective radius. We then calculate the time evolution of the LWP using either the bias corrected ABI during the day or the microwave data, when available, at night. Note that the combined LWP is either directly derived from the microwave imager retrievals or from ABI retrievals that have been corrected to reproduce that same microwave product ensuring consistency across the diurnal cycle.

## 2.5 AMSR-2 Precipitation Rates

We utilize the Advanced Microwave Scanning Radiometer 2 (AMSR-2) warm precipitation product developed by Eastman et al. (2019) to measure changes in precipitation intensity along all trajectories. The product relies on the statistical relationship between  $3 \times 5 \text{ km}^2$  AMSR-2 89-GHz brightness temperatures and collocated CloudSat precipitation rates. Because this dataset cannot precisely discriminate precipitation, we employ a threshold of  $0.1 \text{ mm day}^{-1}$  to distinguish between raining and non-raining AMSR-2 pixels, in a manner similar to Smalley et al. (2022).

Unfortunately, the AMSR-2 data alone cannot be employed to determine how precipitation intensity varies along any single trajectory, as it operates in a sun-synchronous orbit. Therefore, we undertake the following steps: 1) collocate  $1^\circ \times 1^\circ$  unconditionally (including non-precipitating pixels) averaged 2019 AMSR-2 precipitation intensity over the southeast Pacific with GOES-16, and 2) create a lookup table of mean precipitation intensity for a given ABI LWP and ABI  $N_d$  (as shown in Figure S2). Subsequently, we determine the expected precipitation rate at each point by mapping observed ABI LWP and  $N_d$  values back to the lookup table to find the mean precipitation at all time points along all trajectories. Note that this analysis is limited to daytime-only precipitation rates because the ABI LWP and  $N_d$  are unavailable at night.

## 2.6 Cloud Liquid Water Path Sensitivity to initial $N_d$

We assume that any potential changes in  $\lambda$  that may result from entrainment-drying or precipitation suppression are small and might be masked by the diurnal and seasonal cycles in LWP. Therefore, we remove the geographical, seasonal and diurnal cycles (using 2019 – 2021 observations) from LWP (Eq. 2) before calculating  $\lambda$ .

$$CLWP' = \ln(CLWP[\text{time} = t]) - \overline{\ln(CLWP[\text{local hour, month, lat, lon}])} \quad (2)$$

As demonstrated in Figure S3, we calculate  $\lambda[t]$  as the slope of the fit between  $\ln(LWP[t]) - \ln(LWP[t = 0])$  and  $\ln(N_d[t = 0])$ . All estimates of  $\lambda[t]$  are then grouped by initial LWP and averaged to determine how  $\lambda$  varies over time as a function of initial LWP. To reduce noise, we smooth each calculated curve by applying a 6-hour centered running mean.

## 3 Cloud Liquid Water Path Adjustment

Figure 1 demonstrates that, except for the thickest clouds (initial LWP  $> 200 \text{ g m}^{-2}$ ),  $\lambda$  generally tends to be negative, with values decreasing during the day and then increasing at night. Notably the strength of the diurnal cycle of  $\lambda$  is modulated by the initial LWP, with the trajectories with highest LWP, and therefore the greatest tendency to precipitate, having the largest diurnal cycle. While entrainment-drying and precipitation are both likely to maximize during the nighttime hours (Chun et al., 2023), the obvious diurnal cycle suggests a stronger diurnal amplitude of the precipitation suppression mechanism relative to the entrainment-drying mechanism, which results in a near balance in the two processes in the early morning hours for several of the LWP curves. Specifically,  $\lambda$  starts to rise at night and becomes positive in some cases, likely due to stratocumulus thickening and an increased likelihood of intense precipitation (Burleyson et al., 2013). For the highest LWP bin,  $\lambda$  is nearly always positive indicating the dominance of the precipitation suppression mechanism over the entrainment-drying mechanism for these clouds which are most likely to precipitate regardless of time of day.

To quantify the diurnal cycle, Figure 2 displays the autocorrelation function for all  $\lambda$  values shown in Figure 1. Note that linear interpolation was used to fill gaps at night before computing the autocorrelation function (see Figure S4). For the thickest clouds (initial LWP  $> 50 \text{ g m}^{-2}$ ), Figure 2 reveals a statistically significant diurnal cycle, with

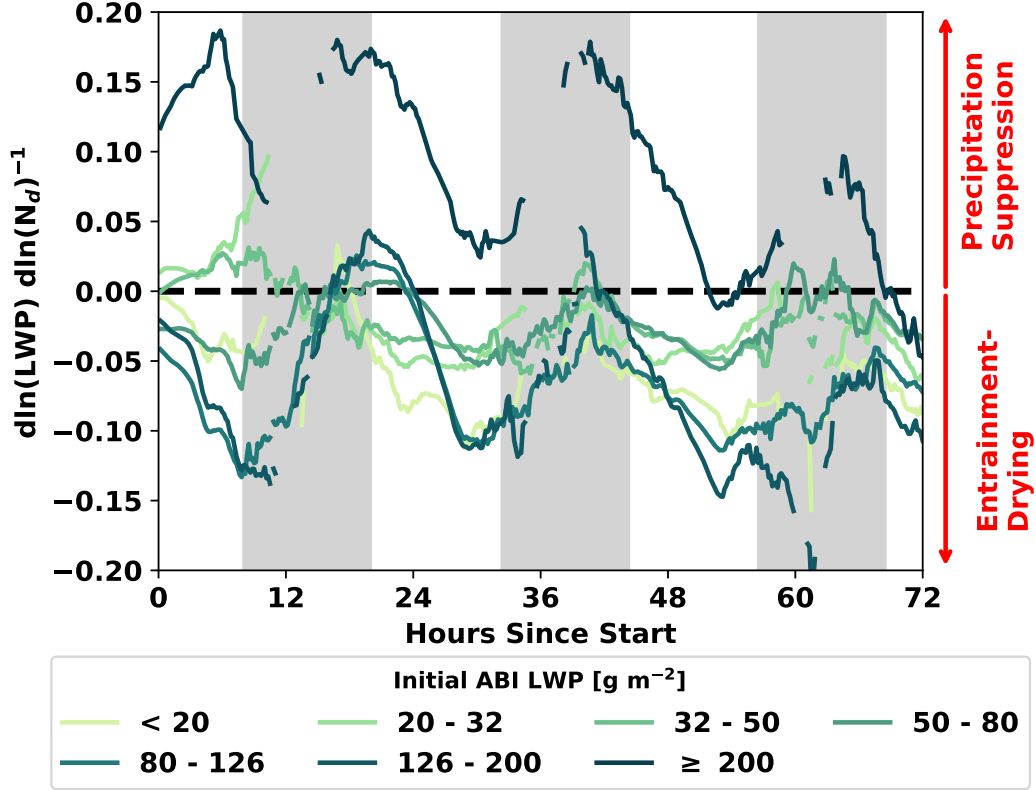


**Figure 1.** The sensitivity in cloud liquid water path (CLWP) to initial cloud-droplet number concentration ( $N_d$ ) conditioned by initial CLWP (line colors). The white-filled regions represent day, and the grey-filled regions represent night.

autocorrelation peaking approximately every 24 hours. For thinner clouds, the autocorrelation drops to zero within 12 hours and does not have a clearly statistically significant diurnal cycle. The sensitivity of the diurnal cycle to LWP strongly suggests that the precipitation suppression process is a critical factor in establishing the diurnal variation in  $\lambda$ .

We have already speculated that the susceptibility of precipitation to aerosol drives the diurnal cycle in  $\lambda$ . Figure 3 substantiates this claim by showing the diurnal (day-time) pattern in precipitation rates binned by LWP. Unsurprisingly there is a strong diurnal cycle in the precipitation rates with a minimum in the late afternoon. However, the amplitude of the diurnal variability increases with initial LWP. Although there is a diurnal cycle in precipitation rates among the thinnest clouds, it is less pronounced com-



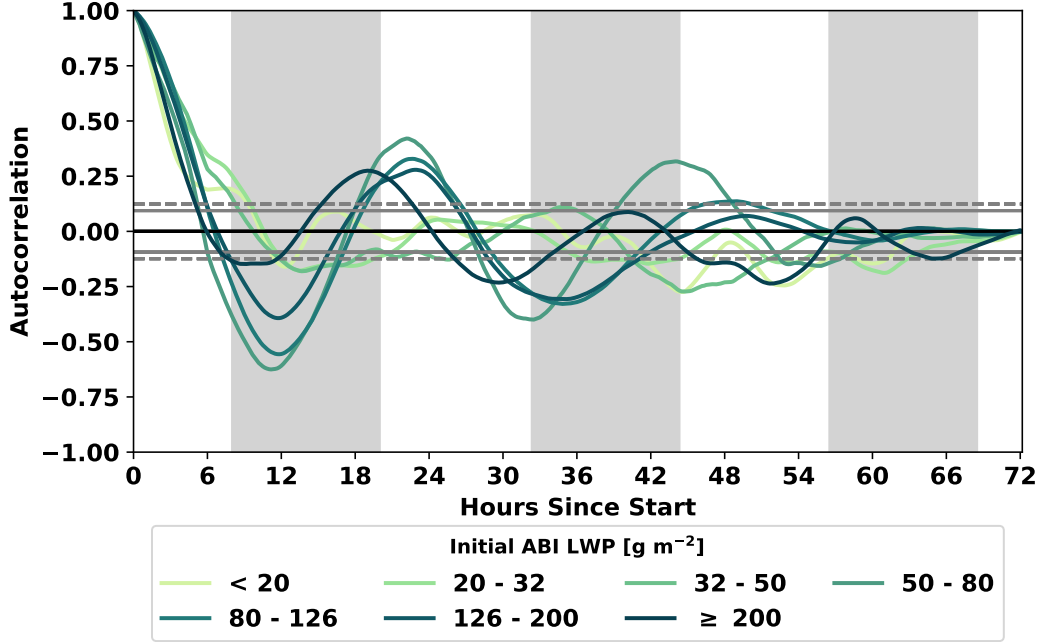


**Figure 2.** The autocorrelation function in the  $\lambda$  curves shown in Figure 1, where each curve represents clouds conditioned by initial CLWP (line colors), where the solid black line represents an autocorrelation of zero, the grey dashed lines represent the 99<sup>th</sup> percentile, and the grey solid lines represent the 95<sup>th</sup> percentile. The white-filled regions represent day, and the grey-filled regions represent night.

pared to the thickest clouds. This, combined with the fact that the thinnest clouds are less likely to produce rainfall (see Figure S2) likely explains the tendency of the diurnal cycle observed in  $\lambda$  to increase with increasing LWP.

#### 4 ABI Cloud Water Path Adjustment Comparison to Prior Studies

As demonstrated in Equation 1, stratocumulus clouds can brighten even when  $\lambda$  is negative. Only a few prior observational (Qiu et al., 2023; Zhou & Feingold, 2023) and LES (Glassmeier et al., 2021) studies have found  $\lambda$  values small enough to darken stratocumulus. Figure 4a compares the mean  $\lambda$  along each composite trajectory with previous studies (Supplemental Table S2). It shows that the mean  $\lambda$  is generally negative for all but the thickest clouds (initial LWP  $> 200 \text{ g m}^{-2}$ ), indicating that entrainment-drying is dominant over precipitation suppression most of the time. While consistent with

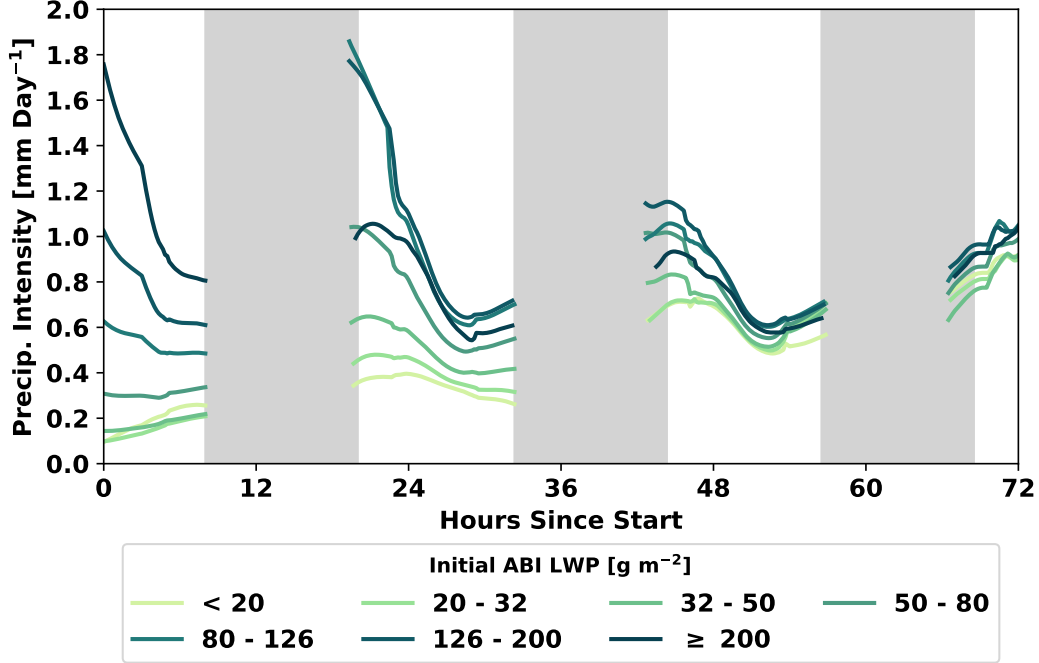


**Figure 3.** The statistical precipitation intensity as determined by using collocated AMSR-2 warm rain rates and GOES-16 ABI CLWP and  $N_d$  (Figure S4) along all trajectories composited by initial ABI CLWP (line colors).

prior studies, our  $\lambda$  values are typically much closer to zero than in most earlier estimates. Specifically we find values of  $\lambda$  that suggest a less significant entrainment-drying mechanism than many prior observational and LES studies.

The diurnal variation of  $\lambda$  suggests that the integrated daytime adjustment should be stronger than the weak overall adjustment shown in Figure 4a. Figure 4b illustrates how the daytime mean  $\lambda$  compares to the mean  $\lambda$  integrated along the full composite trajectories. It reveals that the daytime mean  $\lambda$  is consistently smaller than the full mean  $\lambda$  in all cases. However, even though the negative adjustment appears stronger during the day, it never reaches values indicative of a complete offset of the Twomey effect. The differences between  $\lambda$  calculated from the diurnal vs the daytime only data explain some of the difference between this study and prior studies which are based on daytime observations from visible/near infrared imagery.

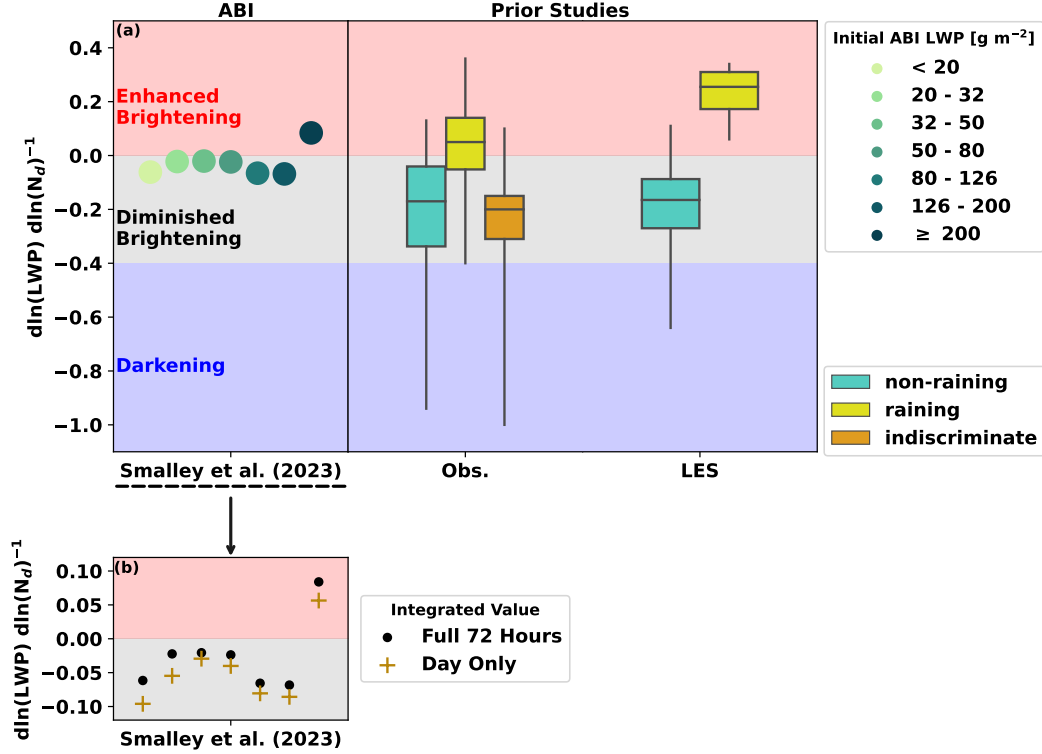


**Figure 4.** Dots (first column) represent the mean  $\lambda$  conditioned along each initial LWP curve shown in Figure 1. Boxplots represent the distribution of  $\lambda$  split between non-raining (turquoise), raining (yellow), and indiscriminate (orange) cases from prior observation-based (second column) and LES (third column) studies. All values are given in table S1. The filled-blue region represents situations where the cloud-field should darken, the grey-filled region represents situations where the cloud-field should brighten despite  $\lambda$  being negative, and the red-filled region represents situations where the cloud-field should brighten.

## 5 Conclusions

Consistent with previous work we find that the sensitivity of stratocumulus LWP to changes in number concentration depends on the initial LWP. Clouds with the largest LWP tend to have a positive sensitivity to increased  $N_d$ , whereas regimes with LWP < about  $200 \text{ g m}^{-2}$  tend to have a negative sensitivity. The difference is presumably related to the dominant mechanism being different for thick clouds (precipitation suppression) and thin clouds (entrainment drying). For analogous reasons, our results emphasize that the adjustment of LWP to increasing aerosol concentrations has a distinct di-

urnal pattern. Throughout the day, we observe a general decrease in  $\lambda$ , with the most negative values occurring late in the afternoon when precipitation is at its lightest. After sunset,  $\lambda$  begins to increase as clouds thicken and precipitation intensity increases. This diurnal variation in  $\lambda$  suggests that while entrainment-drying remains active at night, it is most observable during the day when stratocumulus clouds thin out, and precipitation becomes less frequent and intense. At night, as the stratocumulus deck thickens, the impact of precipitation suppression on  $\lambda$  becomes more pronounced relative to entrainment-drying.

Outside of the stratocumulus clouds most likely to produce the most intense precipitation, the increases in  $\lambda$  at night are insufficient to completely counterbalance the predominantly negative adjustment observed during the day. This typically results in a weak negative adjustment over a period of several days. However, we find that it never reaches magnitudes significant enough to completely offset the Twomey effect.

Our results suggest that marine-cloud brightening is most effective when aerosols are used to seed clouds that are already producing precipitation. This is because the negative impact on LWP in non-precipitating clouds helps counteract the Twomey effect. Furthermore, the significant diurnal cycle in  $\lambda$  implies that the efficacy of any intentional aerosol injection will likely be sensitive to the time of day when it occurs and this dependence will be cloud regime dependent.

## 6 Open Research

GOES-16 Advanced-Baseline Imager cloud optical properties can be downloaded from <https://www.av1.class.noaa.gov>, and ABI liquid water path was corrected using lookup tables available at Zenodo (Smalley & Lebsock, 2023b). The following MERRA-2 products: inst3\_3d\_asm\_Np (Global Modeling and Assimilation Office (GMAO), 2015b) and inst1\_2d\_asm\_Nx (Global Modeling and Assimilation Office (GMAO), 2015a) can be downloaded from the Goddard Space Flight Center Distributed Active Archive Center. Passive Microwave liquid water path can be downloaded from Remote Sensing Systems (<https://www.remss.com>). MODIS Level-2 cloud optical properties can be downloaded from the Level-1 and Atmosphere Archive & Distribution System Distributed Active Archive Center (<https://ladsweb.modaps.eosdis.nasa.gov>). The AMSR-2 warm rain product can be downloaded from the CloudSat Data Processing Center (<https://>

`www.cloudsat.cira.colostate.edu/community-products/warm-rain-rate-estimates`  
`-from-amsr-89ghz-and-cloudsat`). The code used to create and plot the output tra-  
jectory data used in this study are permanently archived at Zenodo (doi: XX.YY.ZZ).

## Acknowledgments

The research was carried out at the Jet Propulsion Laboratory, California Institute of  
Technology, under a contract with the National Aeronautics and Space Administration  
(80NM0018D0004). Ryan Eastman is supported by XX Grant.

## References

- Ackerman, A. S., Kirkpatrick, M. P., Stevens, D. E., & Toon, O. B. (2004). The  
impact of humidity above stratiform clouds on indirect aerosol climate forcing.  
*Nature*, *432*(7020), 1014–1017. doi: 10.1038/nature03174
- Albrecht, B. A. (1989). Aerosols, cloud microphysics, and fractional cloudiness. *Sci-*  
*ence*, *245*(4923), 1227–1230. doi: 10.1126/science.245.4923.1227
- Boers, R., & Mitchell, R. M. (1994). Absorption feedback in stratocumulus clouds:  
Influence on cloud top albedo. *Tellus A*, *46*(3), 229–241. doi: 10.1034/j.1600  
-0870.1994.00001.x
- Bretherton, C. S., Blossey, P. N., & Uchida, J. (2007). Cloud droplet sedimentation,  
entrainment efficiency, and subtropical stratocumulus albedo. *Geophysical Re-*  
*search Letters*, *34*(3). doi: https://doi.org/10.1029/2006GL027648
- Burleyson, C. D., de Szoeke, S. P., Yuter, S. E., Wilbanks, M., & Brewer, W. A.  
(2013). Ship-based observations of the diurnal cycle of southeast pacific marine  
stratocumulus clouds and precipitation. *Journal of the Atmospheric Sciences*,  
*70*(12), 3876–3894. doi: https://doi.org/10.1175/JAS-D-13-01.1
- Christensen, M. W., Jones, W. K., & Stier, P. (2020). Aerosols enhance cloud  
lifetime and brightness along the stratus-to-cumulus transition. *Proceed-*  
*ings of the National Academy of Sciences*, *117*(30), 17591–17598. doi:  
10.1073/pnas.1921231117
- Christensen, M. W., Ma, P.-L., Wu, P., Varble, A. C., Mülmenstädt, J., & Fast,  
J. D. (2023). Evaluation of aerosol–cloud interactions in e3sm using a la-  
grangian framework. *Atmospheric Chemistry and Physics*, *23*(4), 2789–2812.  
doi: 10.5194/acp-23-2789-2023

- 293 Chun, J.-Y., Wood, R., Blossey, P., & Doherty, S. J. (2023). Microphysical, macro-  
294 physical, and radiative responses of subtropical marine clouds to aerosol  
295 injections. *Atmospheric Chemistry and Physics*, 23(2), 1345–1368. Re-  
296 trieved from <https://acp.copernicus.org/articles/23/1345/2023/> doi:  
297 10.5194/acp-23-1345-2023
- 298 Diamond, M. S., Director, H. M., Eastman, R., Possner, A., & Wood, R. (2020).  
299 Substantial cloud brightening from shipping in subtropical low clouds. *AGU*  
300 *Advances*, 1(1), e2019AV000111. doi: 10.1029/2019AV000111
- 301 Diamond, M. S., Gettelman, A., Lebsock, M. D., McComiskey, A., Russell, L. M.,  
302 Wood, R., & Feingold, G. (2022). To assess marine cloud brightening’s tech-  
303 nical feasibility, we need to know what to study—and when to stop. *Pro-*  
304 *ceedings of the National Academy of Sciences*, 119(4), e2118379119. doi:  
305 10.1073/pnas.2118379119
- 306 Douglas, A., & L’Ecuyer, T. (2020). Quantifying cloud adjustments and the radi-  
307 ative forcing due to aerosol–cloud interactions in satellite observations of warm  
308 marine clouds. *Atmospheric Chemistry and Physics*, 20(10), 6225–6241. doi:  
309 10.5194/acp-20-6225-2020
- 310 Eastman, R., Lebsock, M., & Wood, R. (2019). Warm rain rates from amsr-e 89-ghz  
311 brightness temperatures trained using cloudsat rain-rate observations. *Jour-*  
312 *nal of Atmospheric and Oceanic Technology*, 36(6), 1033–1051. doi: [https://doi](https://doi.org/10.1175/JTECH-D-18-0185.1)  
313 [.org/10.1175/JTECH-D-18-0185.1](https://doi.org/10.1175/JTECH-D-18-0185.1)
- 314 Fons, E., Runge, J., Neubauer, D., & Lohmann, U. (2023). Stratocumulus adjust-  
315 ments to aerosol perturbations disentangled with a causal approach. *npj Cli-*  
316 *mate and Atmospheric Science*, 6(1), 130. doi: 10.1038/s41612-023-00452-w
- 317 Glassmeier, F., Hoffmann, F., Johnson, J. S., Yamaguchi, T., Carslaw, K. S., & Fein-  
318 gold, G. (2021). Aerosol-cloud-climate cooling overestimated by ship-track  
319 data. *Science*, 371(6528), 485–489. doi: 10.1126/science.abd3980
- 320 Global Modeling and Assimilation Office (GMAO). (2015a). *inst1\_2d\_asm\_nx: 2d,1-*  
321 *hourly,instantaneous,single-level,assimilation,single-level diagnostics 0.625 x*  
322 *0.5 degree v5.12.4*. Goddard Space Flight Center Distributed Active Archive  
323 Center (GSFC DAAC), Greenbelt, MD, USA. (Accessed January 20, 2023)  
324 doi: 10.5067/3Z173KIE2TPD
- 325 Global Modeling and Assimilation Office (GMAO). (2015b). *inst3\_3d\_asm\_np:*

- 326 *Merra-2 3d, 3-hourly, instantaneous, pressure-level, assimilation, assimilated*  
 327 *meteorological fields v5.12.4 (m2i3npasm)*. Goddard Space Flight Center  
 328 Distributed Active Archive Center (GSFC DAAC), Greenbelt, MD, USA.  
 329 (Accessed January 17, 2023) doi: 10.5067/QBZ6MG944HW0
- 330 Grosvenor, D. P., Sourdeval, O., Zuidema, P., Ackerman, A., Alexandrov, M. D.,  
 331 Bennartz, R., . . . Quaas, J. (2018). Remote sensing of droplet num-  
 332 ber concentration in warm clouds: A review of the current state of knowl-  
 333 edge and perspectives. *Reviews of Geophysics*, 56(2), 409–453. doi:  
 334 <https://doi.org/10.1029/2017RG000593>
- 335 Gryspeerdt, E., Glassmeier, F., Feingold, G., Hoffmann, F., & Murray-Watson, R. J.  
 336 (2022). Observing short-timescale cloud development to constrain aerosol–  
 337 cloud interactions. *Atmospheric Chemistry and Physics*, 22(17), 11727–11738.  
 338 doi: 10.5194/acp-22-11727-2022
- 339 Hill, A. A., Feingold, G., & Jiang, H. (2009). The influence of entrainment and mix-  
 340 ing assumption on aerosol–cloud interactions in marine stratocumulus. *Journal*  
 341 *of the Atmospheric Sciences*, 66(5), 1450–1464. doi: [https://doi.org/10.1175/](https://doi.org/10.1175/2008JAS2909.1)  
 342 [2008JAS2909.1](https://doi.org/10.1175/2008JAS2909.1)
- 343 Hoffmann, F., & Feingold, G. (2021). Cloud microphysical implications for  
 344 marine cloud brightening: The importance of the seeded particle size dis-  
 345 tribution. *Journal of the Atmospheric Sciences*, 78(10), 3247–3262. doi:  
 346 [10.1175/JAS-D-21-0077.1](https://doi.org/10.1175/JAS-D-21-0077.1)
- 347 Hu, Y., Lu, X., Zhai, P.-W., Hostetler, C. A., Hair, J. W., Cairns, B., . . . Wood,  
 348 R. (2021). Liquid phase cloud microphysical property estimates from  
 349 calipso measurements. *Frontiers in Remote Sensing*, 2. Retrieved from  
 350 <https://www.frontiersin.org/articles/10.3389/frsen.2021.724615>  
 351 doi: 10.3389/frsen.2021.724615
- 352 Lebsock, M. D., Stephens, G. L., & Kummerow, C. (2008). Multisensor  
 353 satellite observations of aerosol effects on warm clouds. *Journal of Geo-*  
 354 *physical Research: Atmospheres*, 113(D15). Retrieved from [https://](https://agupubs.onlinelibrary.wiley.com/doi/abs/10.1029/2008JD009876)  
 355 [agupubs.onlinelibrary.wiley.com/doi/abs/10.1029/2008JD009876](https://agupubs.onlinelibrary.wiley.com/doi/abs/10.1029/2008JD009876) doi:  
 356 <https://doi.org/10.1029/2008JD009876>
- 357 Lee, S. S., Penner, J. E., & Saleeby, S. M. (2009). Aerosol effects on liquid-water  
 358 path of thin stratocumulus clouds. *Journal of Geophysical Research: Atmo-*

- spheres, 114(D7). doi: <https://doi.org/10.1029/2008JD010513>
- Michibata, T., Suzuki, K., Sato, Y., & Takemura, T. (2016). The source of discrepancies in aerosol–cloud–precipitation interactions between gcm and a-train retrievals. *Atmospheric Chemistry and Physics*, 16(23), 15413–15424. doi: 10.5194/acp-16-15413-2016
- Mülmenstädt, J., & Feingold, G. (2018). The radiative forcing of aerosol–cloud interactions in liquid clouds: Wrestling and embracing uncertainty. *Current Climate Change Reports*, 4(1), 23–40. doi: 10.1007/s40641-018-0089-y
- Pavolonis, M. (2020). *Enterprise algorithm theoretical basis document for cloud type and cloud phase* (NOAA Tech. Rep. No. 113 pp). NOAA. Retrieved from [https://www.star.nesdis.noaa.gov/goesr/rework/documents/ATBDs/Enterprise/Enterprise\\_ATBD\\_Cloud\\_CldType\\_G17\\_Mitigation\\_Jun2020.pdf](https://www.star.nesdis.noaa.gov/goesr/rework/documents/ATBDs/Enterprise/Enterprise_ATBD_Cloud_CldType_G17_Mitigation_Jun2020.pdf)
- Platnick, S., Ackerman, S. A., King, M. D., Meyer, K., Menzel, W. P., Holz, R. E., ... Yang, P. (2015). *Modis atmosphere l2 cloud product (06\_l2)*. NASA MODIS Adaptive Processing System, Goddard Space Flight Center. (Last accessed: September 26, 2023) doi: [dx.doi.org/10.5067/MODIS/MOD06\\_L2.006](https://dx.doi.org/10.5067/MODIS/MOD06_L2.006)
- Platnick, S., & Twomey, S. (1994). Determining the susceptibility of cloud albedo to changes in droplet concentration with the advanced very high resolution radiometer. *Journal of Applied Meteorology and Climatology*, 33(3), 334–347. doi: 10.1175/1520-0450(1994)033<0334:DTSOCA>2.0.CO;2
- Prabhakaran, P., Hoffmann, F., & Feingold, G. (2023). Evaluation of pulse aerosol forcing on marine stratocumulus clouds in the context of marine cloud brightening. *Journal of the Atmospheric Sciences*, 80(6), 1585–1604. doi: <https://doi.org/10.1175/JAS-D-22-0207.1>
- Qiu, S., Zheng, X., Painemal, D., Terai, C., & Zhou, X. (2023). Diurnal variation of aerosol indirect effect for warm marine boundary layer clouds in the eastern north atlantic. *EGUsphere*, 2023, 1–30. doi: 10.5194/egusphere-2023-1676
- Sandu, I., Brenguier, J. L., Geoffroy, O., Thouron, O., & Masson, V. (2008). Aerosol impacts on the diurnal cycle of marine stratocumulus. *Journal of the Atmospheric Sciences*, 65(8), 2705–2718. doi: <https://doi.org/10.1175/2008JAS2451.1>
- Seinfeld, J. H., Bretherton, C., Carslaw, K. S., Coe, H., DeMott, P. J., Dunlea,



- 392 E. J., ... Wood, R. (2016). Improving our fundamental understand-  
393 ing of the role of aerosol-cloud interactions in the climate system. *Pro-*  
394 *ceedings of the National Academy of Sciences*, 113(21), 5781–5790. doi:  
395 10.1073/pnas.1514043113
- 396 Smalley, K. M., & Lebsock, M. (2023b). *Corrections for geostationary cloud liquid*  
397 *water path using microwave imagery (1.0.0) [data set]*. Zenodo. (Last accessed:  
398 November 7, 2023) doi: 10.5281/zenodo.7647786
- 399 Smalley, K. M., & Lebsock, M. D. (2023a). Corrections for geostationary cloud liq-  
400 uid water path using microwave imagery. *Journal of Atmospheric and Oceanic*  
401 *Technology*, 40(9), 1049-1061. doi: <https://doi.org/10.1175/JTECH-D-23-0030>  
402 .1
- 403 Smalley, K. M., Lebsock, M. D., Eastman, R., Smalley, M., & Witte, M. K.  
404 (2022). A lagrangian analysis of pockets of open cells over the southeast-  
405 ern pacific. *Atmospheric Chemistry and Physics*, 22(12), 8197-8219. doi:  
406 10.5194/acp-22-8197-2022
- 407 Toll, V., Christensen, M., Quaas, J., & Bellouin, N. (2019). Weak average liquid-  
408 cloud-water response to anthropogenic aerosols. *Nature*, 572(7767), 51–55. doi:  
409 10.1038/s41586-019-1423-9
- 410 Twomey, S. (1977). The influence of pollution on the shortwave albedo of  
411 clouds. *Journal of Atmospheric Sciences*, 34(7), 1149–1152. doi: 10.1175/  
412 1520-0469(1977)034(1149:TIOPOT)2.0.CO;2
- 413 Walther, A., & Straka, W. (2020). *Algorithm theoretical basis document for daytime*  
414 *cloud optical and microphysical properties (dcomp)* (NOAA Tech. Rep. No. 64  
415 pp). NOAA. Retrieved from [https://www.star.nesdis.noaa.gov/goesr/](https://www.star.nesdis.noaa.gov/goesr/documents/ATBDs/Enterprise/ATBD_Enterprise_Daytime_Cloud_Optical_and_Microphysical_Properties(DCOMP)_v1.2_2020-10-09.pdf)  
416 [documents/ATBDs/Enterprise/ATBD\\_Enterprise\\_Daytime\\_Cloud\\_Optical](https://www.star.nesdis.noaa.gov/goesr/documents/ATBDs/Enterprise/ATBD_Enterprise_Daytime_Cloud_Optical_and_Microphysical_Properties(DCOMP)_v1.2_2020-10-09.pdf)  
417 [\\_and\\_Microphysical\\_Properties\(DCOMP\)\\_v1.2\\_2020-10-09.pdf](https://www.star.nesdis.noaa.gov/goesr/documents/ATBDs/Enterprise/ATBD_Enterprise_Daytime_Cloud_Optical_and_Microphysical_Properties(DCOMP)_v1.2_2020-10-09.pdf)
- 418 Wentz, F. J. (1997). A well-calibrated ocean algorithm for special sensor mi-  
419 crowave/imager. *Journal of Geophysical Research: Oceans*, 102(C4), 8703-  
420 8718. doi: <https://doi.org/10.1029/96JC01751>
- 421 Wentz, F. J., & Spencer, R. W. (1998). Ssm/i rain retrievals within a unified all-  
422 weather ocean algorithm. *Journal of the Atmospheric Sciences*, 55(9), 1613-  
423 1627. doi: [https://doi.org/10.1175/1520-0469\(1998\)055\(1613:SIRRWA\)2.0.CO;](https://doi.org/10.1175/1520-0469(1998)055(1613:SIRRWA)2.0.CO;2)  
424 2

- 425 Wood, R. (2021). Assessing the potential efficacy of marine cloud brightening for  
 426 cooling earth using a simple heuristic model. *Atmospheric Chemistry and*  
 427 *Physics*, 21(19), 14507–14533. doi: 10.5194/acp-21-14507-2021
- 428 Wood, R., & Bretherton, C. S. (2006). On the relationship between stratiform low  
 429 cloud cover and lower-tropospheric stability. *Journal of Climate*, 19(24), 6425  
 430 - 6432. Retrieved from [https://journals.ametsoc.org/view/journals/](https://journals.ametsoc.org/view/journals/clin/19/24/jcli3988.1.xml)  
 431 [clin/19/24/jcli3988.1.xml](https://journals.ametsoc.org/view/journals/clin/19/24/jcli3988.1.xml) doi: <https://doi.org/10.1175/JCLI3988.1>
- 432 Zhou, X., & Feingold, G. (2023). Impacts of mesoscale cloud organization on  
 433 aerosol-induced cloud water adjustment and cloud brightness. *Geophysical*  
 434 *Research Letters*, 50(13), e2023GL103417. doi: 10.1029/2023GL103417